Self-Enhanced Ligand Degradation Underlies Robustness of Morphogen Gradients

Avigdor Eldar,[1,2] Dalia Rosin,[1]
Ben-Zion Shilo,[1] and Naama Barkai[1,2,*]
[1]Department of Molecular Genetics
[2]Department of Physics of Complex Systems
Weizmann Institute of Science
Rehovot 76100
Israel

Summary

Morphogen gradients provide long-range positional information by extending across a developing field. To ensure reproducible patterning, their profile is invariable despite genetic or environmental fluctuations. Common models assume a morphogen profile that decays exponentially. Here, we show that exponential profiles cannot, at the same time, buffer fluctuations in morphogen production rate and define long-range gradients. To comply with both requirements, morphogens should decay rapidly close to their source but at a significantly slower rate over most of the field. Numerical search revealed two network designs that support robustness to fluctuations in morphogen production rate. In both cases, morphogens enhance their own degradation, leading to a higher degradation rate close to their source. This is achieved through reciprocal interactions between the morphogen and its receptor. The two robust networks are consistent with properties of the Wg and Hh morphogens in the *Drosophila* wing disc and provide novel insights into their function.

Introduction

Morphogens are signaling molecules that induce distinct cell fates at different concentrations. During development, gradients of morphogens provide long-range positional information for patterning tissues and organs (Wolpert, 1989). Among the signaling molecules implicated as morphogens are growth factors of the TGF-β, Wingless (Wg), and Hedgehog (Hh) families (Briscoe and Ericson, 2001; Chuang and Kornberg, 2000; Lecuit and Cohen, 1997; McDowell and Gurdon, 1999; Nellen et al., 1996; Neumann and Cohen, 1997a; Roelink et al., 1995). Those molecules are involved in numerous patterning events, but their function was studied most extensively in the *Drosophila* wing disc (Lecuit et al., 1996; Neumann and Cohen, 1997b; Strigini and Cohen, 1997; Zecca et al., 1996). Recently, the distribution of Dpp (a TGF-β homolog) and Wg in the wing disc was visualized directly, demonstrating their ability to rapidly form long-range gradients that extend throughout the wing disc (Entchev et al., 2000; Strigini and Cohen, 2000; Teleman and Cohen, 2000).

The pattern of gene expression induced by morphogen gradients depends on the quantitative levels of the ligand across the developing field, since boundaries between cell fates are established at particular thresholds. However, the morphogen is produced only at a spatially restricted source, and the rate of its production may vary due to genetic alterations or fluctuations in temperature or nutrients. Yet, a reliable pattern is established despite such fluctuations. Temporal averaging could provide one mechanism for buffering fluctuations in gene expression. However, such a mechanism would not apply to cases of persistent changes, such as alteration in gene dosage. In the *Drosophila* wing imaginal disc, for example, it was shown that intermediate increase in Dpp expression has little effect on wing and thorax patterning (Morimura et al., 1996). While similar experiments were not yet done for Wg and Hh morphogens, it is known that wing patterning is precise in heterozygous mutants that have only one functional allele of Hh or Wg.

An emerging theme is that feedback mechanisms play a prominent role in shaping morphogen gradients (Freeman, 2000; Perrimon and McMahon, 1999). Regulatory mechanisms were identified at all levels of morphogen function, including movement away from the source (Bellaiche et al., 1998; Burke et al., 1999; Chen and Struhl, 1996), stability (Cadigan et al., 1998; Gerlitz and Basler, 2002; Giraldez et al., 2002), and the sensitivity of the receiving cells to morphogen signaling (Campbell and Tomlinson, 1999; Jazwinska et al., 1999). Recently, the roles of receptors in shaping morphogen gradients received much interest. Theoretical analysis demonstrated that high binding affinities may hinder ligand diffusion, but biologically relevant gradients can still be formed by diffusion, when receptor-mediated ligand degradation is taken into account (Kerszberg and Wolpert, 1998; Lander et al., 2002). Feedback regulation of receptor expression was identified for all three morphogens patterning the *Drosophila* wing disc (Cadigan, 2002; Strigini and Cohen, 1999). In the Wg and Hh systems, it was also shown that receptors modify the stability, or the range of action of their ligands (Cadigan et al., 1998; Chen and Struhl, 1996). Regulated ligand degradation is also involved in shaping the Wg gradient in *Drosophila* embryo (Dubois et al., 2001). However, how such feedback retains the precise shape of the morphogen gradient is not yet understood.

In this work, we propose a general mechanism for achieving robustness of morphogen gradients. We find that rapid decay of morphogen distribution close to the source is required for buffering fluctuations in the rate of morphogen production, while more gradual decay further away from the source allows sufficient ligand levels to reach distant cells. A numerical screen revealed two designs of morphogen networks that support robustness. In both cases, the regulatory interaction between morphogens and their cognate receptors leads to enhanced morphogen degradation close to the source where morphogen levels are high. Detailed analysis suggests that those network designs are employed during

*Correspondence: naama.barkai@weizmann.ac.il

Drosophila wing disc patterning by the Wg and Hh morphogens. Novel insights and predictions regarding molecular properties of those systems are described. In particular, our model proposes that the stabilization of Wg by its receptor DFz2 requires active interference of DFz2 with the degradation of free Wg. We provide experimental evidence supporting this prediction.

Results

Theory: Interplay between Long-Range Gradient and Robustness

In most morphogen systems, the secretion of ligands from a localized source initiates the patterning process. The rate by which morphogen is produced is determined only at the source, but its spread defines patterning throughout the developing field. It is thus important to ensure that possible changes in the rate of morphogen production will not alter morphogen levels across the field. An additional, seemingly unrelated requirement is that a morphogen will spread to sufficient distances from the source. Below, we examine theoretically different morphogen profiles in view of those two constraints.

Our analysis focuses on the shape of the morphogen gradient itself. In all pathways, intracellular transduction from the ligand to the nucleus involves multiple components and feedback loops. However, since the level of signaling is a direct outcome of the local external ligand concentration, feedbacks which do not affect this distribution cannot be utilized to buffer against fluctuations in morphogen profiles. Rather, in a naive tissue, a shift in the morphogen profile will induce a corresponding shift in the signaling curve, irrespective of the downstream transduction mechanisms.

In the simplest class of models, morphogens are described as extracellular diffusable molecules undergoing linear degradation. Morphogen distribution approaches a steady-state profile which decays exponentially with a characteristic decay length, λ, that depends on both the diffusion constant D and the degradation rate α with

$$\lambda = \sqrt{D/\alpha}$$

(Figure 1A). This single decay length reflects the uniform decay of morphogen: its concentration decreases by a fixed ratio between any two points that are separated by a given distance, irrespective of their absolute distance from the source.

Consider two cell fate boundaries established at positions x_1 and x_2. The distance between those two positions,

$$\Delta x = (x_2 - x_1),$$

is given in terms of the morphogen concentrations c_1 and c_2, which define the respective thresholds for cell fate induction:

$$\Delta x = \lambda \log(c_1/c_2). \tag{1}$$

Thus, in order to induce several cell fates, λ should be comparable to the size of the developing field. For example, morphogen decreases 10-fold over a distance

$$\Delta x \cong 2.3\lambda$$

and 1000-fold over a distance

$$\Delta x \cong 7\lambda.$$

Suppose that the rate of morphogen production fluctuates between its normal value, η_1, and an altered value, η_2. Those fluctuations modify the morphogen levels everywhere, causing a uniform shift δx in cell fate boundaries:

$$\delta x = \lambda \log(\eta_1/\eta_2). \tag{2}$$

Thus, the extent of shift in cell fate boundary is of the order of the morphogen decay length λ. Robustness requires fast morphogen decay, corresponding to small λ. However, such fast decay would preclude morphogen from extending across the field (see Equation 1). We conclude that, when considering exponentially distributed morphogen gradients, the interplay between robustness and long-range patterning poses a fundamental problem.

To see how this inherent difficulty can be overcome, we considered a general model of a single morphogen diffusing in a naive field (Supplemental Data, section 1, available online at http://www.developmentalcell.com/cgi/content/full/5/4/635/DC1). Also in this general model, fluctuation in the rate of morphogen production will cause a uniform shift of all boundaries by the same extent δx, irrespective of their absolute distance from morphogen source, with

$$\delta x \approx \frac{dx}{d \ln c(x)}\bigg|_{x=0} \tag{3}$$

(see Supplemental Data, section 1.3 for derivation). Since the derivative in the above equation is calculated at $x = 0$, robustness is enhanced with increasing rate of morphogen decay in the vicinity of the source but does not depend on the rate of morphogen decay elsewhere in the field. We conclude that to comply with both requirements (high buffering capacity and long diffusion range), morphogen profiles should decay rapidly close to the source but at a lower rate across most of the field.

Differential decay rates are obtained naturally when a morphogen undergoes nonlinear, rather than linear, degradation (Figure 1B). In this case, the steady-state morphogen profile is given by (see Supplemental Data, section 1.5)

$$c(x) = \frac{A}{(x + \epsilon)^m}; \tag{4}$$

with $\epsilon \propto \eta^{-\gamma}$. The parameters $y > 0$, A, and m are defined by system-specific properties (but do not depend on η, see Supplemental Data section 1.5). Note that this profile decays rapidly close to morphogen source, but its decay rate decreases with increasing distance from the source. In the limit of large η, the profile becomes independent of morphogen production rate, so that fluctuations in this rate will not alter the cell fate boundaries, leading to
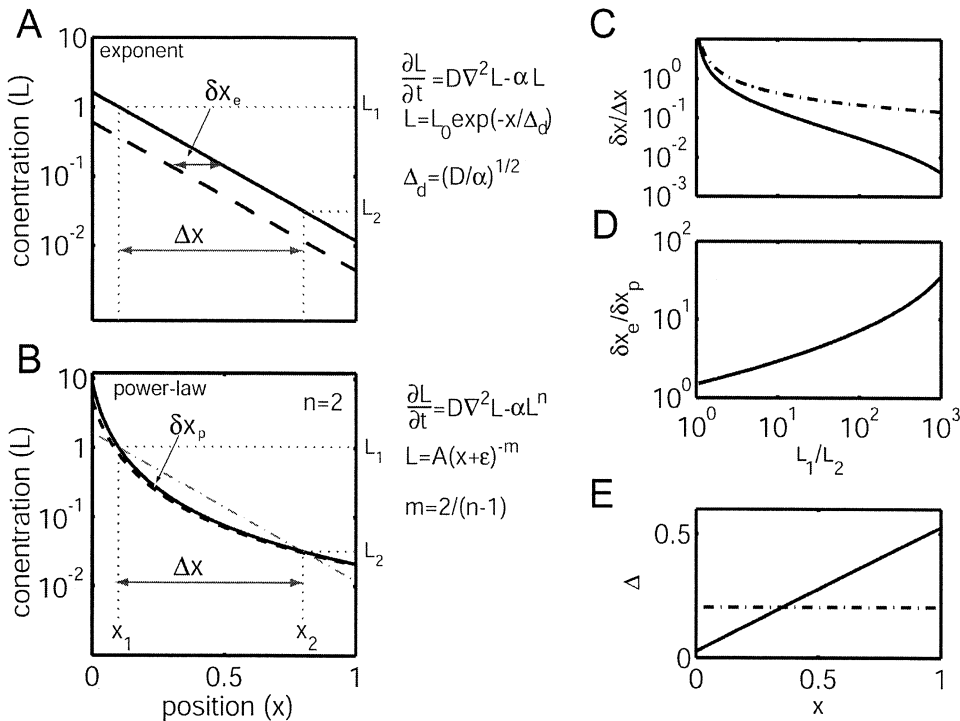
Figure 1. Properties of Exponential versus Power-Law Morphogen Profiles

(A) A diffusible morphogen that is subject to linear degradation approaches an exponential profile at steady state (solid line). A perturbed profile (dashed line) was obtained by reducing the morphogen production rate (η) by a factor e. The resulting shift in cell fate boundary (δx_e) is comparable to the distance between two boundaries in the unperturbed profile (Δx). Note the logarithmic scale.

(B) When morphogen undergoes nonlinear degradation, a power-law morphogen profile is established at steady state. In this case, ∂x_p is significantly smaller than Δx. The symbols are the same as in (A), and $n = 2$. See Supplemental Data for the expressions of A and ϵ. For comparison, the exponential distribution (solid line in [A]) is also shown (dashed-dotted line).

(C) The sensitivity of morphogen profile to fluctuations in morphogen production rate was measured by the ratio $\delta x/\Delta x$. This measure is plotted as a function of the fold decrease in morphogen concentration L_1/L_2. Dashed-dotted line corresponds to exponential profile and solid line to power-law distribution.

(D) The ratio between the sensitivity of an exponential profile to that of a power-law profile, $\partial x_e/\partial x_p$, as a function of L_1/L_2.

(E) The rate of morphogen decay is defined as $d\ln(P(x))/dx$, with $P(x)$ denoting the morphogen distribution. Plotted here is the degradation length (Δ), defined as the inverse of this decay, as a function of the distance from the source, for exponential (dashed-dotted) and power-law (black) profiles. Note that the degradation length is uniform for exponential profiles, but increases with increasing distance from the source for power-law profiles.

In (A) and (B), $x_1 = 0.2$, $x_2 = 0.6$, $L_1 = 1$, $L_2 = 0.01$. In (C) and (D), $x_1 = 0.03$, $x_2 = 0.9$.

$$\delta x \cong 0. \qquad (5)$$

Nonlinear morphogen degradation thus ensures robustness to fluctuations in the rate of morphogen production. When degradation is nonlinear, increasing morphogen production enhances morphogen degradation specifically close to the source where morphogen accumulates. Such differential control of the rate of morphogen degradation (close to the source and away from it) is not possible in the case of exponential profiles.

Numeric Screen for Robust Morphogen Networks
General Model of Morphogen Systems
We examined the applicability of the general theory to possible molecular designs of morphogen networks. Several aspects are required for establishing morphogen gradients: secretion of morphogen from a localized source, morphogen diffusion (or nondirectional transport) across the developing field, and morphogen degradation. In addition, receptor binding is needed for transducing the morphogen signals. As a starting point for

identifying robust patterning mechanisms, we formulated a general model of a morphogen which incorporates those four aspects, outlined in Figure 2 (see Experimental Procedures and Supplemental Data section 2 for mathematical formulation).

The relative importance of each interaction in the model is characterized by an associated rate constant. A concrete realization of a network, obtained by assigning actual values to all biochemical parameters, corresponds to a specific molecular mechanism. Our analysis does not make a priori assumptions regarding the dominant interactions, since in the typical reference system we are giving comparable weights to all interactions at the outset.
Numerical Screen for Robust Networks
We employed a numerical screen to identify robust networks. A large set of networks with different realization of parameters was considered, and the capacity of each network to buffer fluctuations in the rate of morphogen production was evaluated. This was done by choosing each parameter at random out of a distribution that was
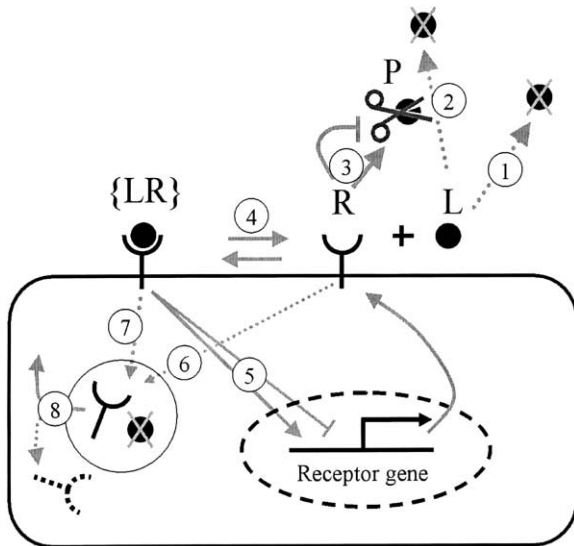
Figure 2. Reactions Included in the Numerical Screen

A morphogen network composed of three components: the ligand (L), receptor (R), and a protease (P) degrading the ligand. Ligand can bind the receptor (4). It is degraded by protease (2) or through receptor-mediated endocytosis (7) in addition to passive loss (1). Protease levels are regulated (either positively or negatively) by the free receptor (3). The receptor expression is transcriptionally regulated (enhanced or repressed) by morphogen signaling (5). Free receptor can be endocytosed (6), followed by its degradation or recycling back to the membrane (8).

centered at a reference system and ranged over four orders of magnitude. To quantify the robustness of each network, we considered an arbitrary cell fate boundary in the middle of the field. The level of morphogen at this point defines a network-specific threshold for gene expression. Robustness was measured by reducing morphogen levels 2-fold and measuring the resulting shift in cell fate boundary. For example, the position of the threshold in the nonrobust profile in Figure 3B is shifted by 15% upon 2-fold reduction of ligand secretion rate, as expected for an exponential profile. The majority of systems displayed a similar sensitivity. A small fraction of networks ($<$1%) were identified as robust, displaying a significantly smaller sensitivity than exponential profiles. For example, the threshold in the robust system in Figure 3B is shifted by less than 5% upon 2-fold reduction of ligand secretion rate.

Properties of Robust Networks

In the majority of networks, morphogen distribution approached an exponential profile. In sharp contrast, none of the robust networks generated an exponential shape. Rather, the robust profiles were characterized by a rapid decay in the vicinity of the morphogen source and a significantly slower decay elsewhere (Figure 3C). This result is in agreement with the general theoretical discussion presented above.

We studied design features of the robust networks by comparing statistical properties of the parameters found in the robust versus nonrobust cases. In most (over 90%) of the nonrobust networks, morphogen was degraded linearly. In sharp contrast, virtually none of the robust

networks relied on such linear degradation (Figure 3D). Rather, the robust networks could be classified into two distinct classes based on the morphogen degradation mechanism (Figures 3E and 3F). In networks of the first class, morphogen was degraded primarily by a protease which, in turn, was negatively regulated by the receptor. In the second class, morphogen was degraded primarily by receptor-mediated endocytosis. Receptor expression was regulated by morphogen signaling in both classes, exhibiting downregulation in the first case and upregulation in the second.

Robustness in Patterning the Drosophila *Wing Imaginal Disc*

To investigate the applicability of our analysis to patterning of actual biological systems, we focused on the *Drosophila* wing imaginal disc. We first considered the possible role of heparan sulfate proteoglygans (HSPGs), which are known to play a role in wing disc patterning (but were not included in our general model), in providing robustness. Subsequently, we present evidence that the two robust network designs identified by our numerical screen resemble interactions found in the Wg and Hh systems during wing disc patterning. We denote those classes as Wg-like and Hh-like and discuss the implication of this analogy to wing disc patterning.

Morphogen-HSPG Interactions

The key result of our theoretical analysis (see above, section 1 of Results), is that in order to obtain a morphogen gradient that robustly establishes multiple thresholds, the morphogen profile should decay rapidly close to its source but at lower rates further away from it. Morphogen decay length represents a balance between morphogen diffusion and degradation. While robustness could be achieved by modulating either of the two, the solutions which emerged from the numerical screen affect only morphogen degradation. Extracellular factors, such as HSPGs, that play an important role in wing disc patterning were not included in our general model. This class of protein/polysaccharide macromolecules resides on the cell surface and binds extracellular ligands. We thus asked if regulation of HSPGs could also be used to achieve robustness.

We examined how morphogen spread may be affected by reversible binding to HSPGs. We found that the steady-state distribution of free morphogen is not affected by such binding, although the time to reach steady state is increased (see Supplemental Data). Consequently, modulating the local levels of HSPG-morphogen binding sites will not alter the steady-state profile of free morphogen. We conclude that since robustness depends only on the level of free morphogen, regulation of ligand binding to HSPGs cannot be used as a mechanism for achieving robustness.

It should be noted, however, that HSPGs affect morphogen signaling by a variety of modes. Putative mechanisms by which HSPGs may contribute to robustness could be envisioned. For example, HSPGs could alter the degradation of free morphogen, either directly or through the presentation of ligand to the receptor. Alternatively, HSPGs may actively facilitate morphogen diffusion, e.g., by transferring morphogen between the
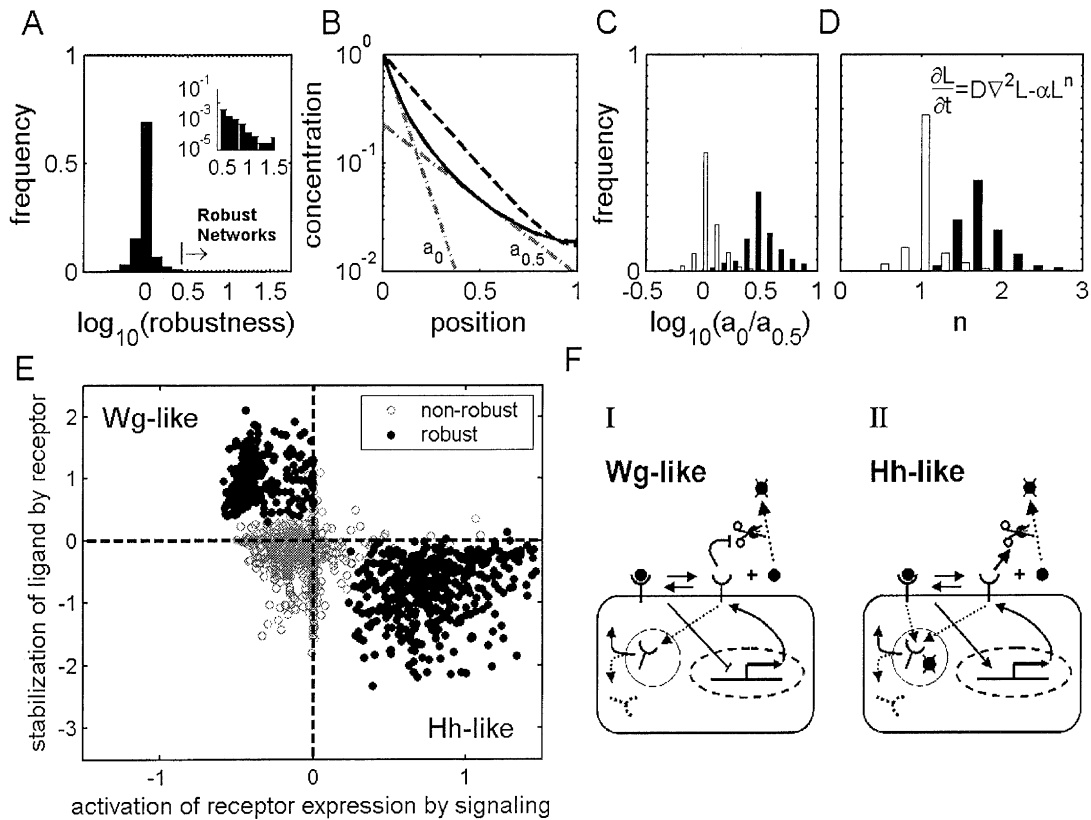
Figure 3. Properties of Robust Networks Identified by the Numerical Screen

(A) Distribution of the extent of robustness displayed by the 100,000 networks simulated. Robustness was measured relative to that of an equivalent exponential profile (see Experimental Procedures and Supplemental Data). Ninety-seven percent of the systems are exponential-like with robustness of ~1. A small fraction of the networks (<1%) exhibited a significantly higher robustness (inset). The arrow indicates the threshold beyond which a network was included in the class of robust networks. Note the logarithmic scale.

(B) Typical profiles of robust (solid line) and nonrobust (dashed line) networks. The dashed-dotted lines emphasize the distinct decay rates of the robust profile at $x = 0$ and $x = 0.5$.

(C) Ratio of the decay length at $x = 0.5$ and at $x = 0$, for the robust (solid bars) and nonrobust (open bars) networks. In all robust cases, the length scale at $x = 0$ is significantly smaller than at $x = 0.5$, indicating a more rapid decay close to the source. In contrast, the nonrobust networks decay at a similar rate everywhere.

(D) The nonlinearity of morphogen degradation can be described by the power-law (n) defining the decay of the profile close to the source. Shown are the values of this power for the robust (solid bars) and nonrobust (open bars) networks. Note that $n > 1$ in all robust cases, indicating nonlinear morphogen degradation close to the source.

(E) Design properties of the robust networks. Each of the robust networks is indicated by a closed circle. Its position along the x axis is according to the extent by which signaling induces receptor expression (positive values corresponding to upregulation, negative values to downregulation, while $x = 0$ indicates no transcription feedback). Its position along the y axis is according to the extent by which receptor enhances ligand degradation (positive values indicated enhanced stabilization, negative values enhanced degradation, while $y = 0$ indicates no effect). For comparison, a similar number (730) of nonrobust networks is also shown (open gray circles). Note that the nonrobust networks are concentrated close to the origin.

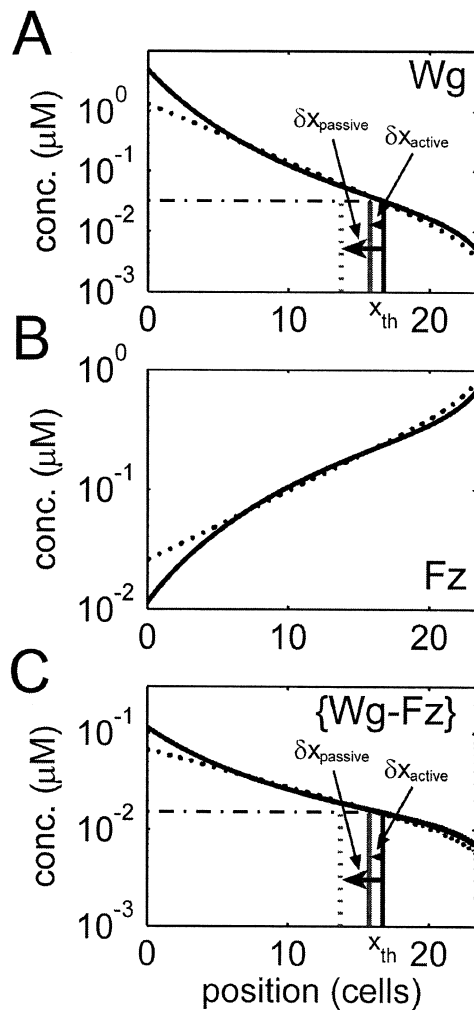(F) The design features characterizing the two classes of robust networks.

attached polysaccharide chains. When experimental indications for such mechanisms arise, it will be interesting to examine further their contribution to robust patterning.

Wg-DFz2 Interaction in the Drosophila Wing Disc

Wg is produced by two cell rows in the dorsoventral boundary of the wing disc. The shape of the Wg gradient is affected by interactions with its principle receptor, DFz2 (Cadigan et al., 1998; Rulifson et al., 2000). Overexpression of DFz2 increases the net levels of Wg, as judged by whole-disc Western blots, and leads to accumulation of Wg on the surface of the overexpressing cells. It was also reported that DFz2 expression is repressed at regions of high Wg signaling (Cadigan et al., 1998; Lecourtois et al., 2001). Indeed, those two features, Wg stabilization by its receptor and downregulation of receptor expression by Wg signaling, characterize the Wg-like class of robust networks identified in our numerical screen.

Stabilization of Wg by DFz2 could be due to passive protection, namely by sequestration of the receptor-bound Wg from degradation. Alternatively, it could also stem from active interference of DFz2 with the degradation of free Wg, e.g., by sequestering or inhibiting a

Figure 4. Active Ligand Stabilization Confers Robustness

Numerical simulation comparing passive protection (dotted line) and active stabilization (solid line). In both models, the binding of ligand to receptor prevents its degradation, while morphogen signaling represses the expression of its receptor. However, only in the second model does the receptor also reduce the degradation rate of free (unbound) ligand by sequestering a putative protease. Shown are the concentration of morphogen (A), receptor (B), and the complex ligand-receptor (C). The shift in cell fate boundary following a 3-fold decrease in morphogen levels is indicated in (A) and (C) ($\delta x_{passive}$ for passive protection, and δx_{active} for active stabilization). See Supplemental Data, section 3 for equations and parameters.

putative protease. Our analysis makes a clear distinction between those two alternative mechanisms: in all networks assigned to the Wg-like class, the receptor reduces free Wg degradation through active stabilization, which is required for achieving robustness (Figure 4). Previous reports, however, attributed Wg stabilization to its passive protection by DFz2 (Cadigan et al., 1998; Rulifson et al., 2000).

Experimental Support for Active Stabilization of Wg by DFz2

A central issue is how to examine experimentally the involvement of active ligand stabilization, since a graded morphogen profile is obtained in the presence of either active stabilization or passive protection. We have used computer simulation to examine the expected Wg accumulation upon ectopic expression of DFz2 in a stripe that is perpendicular to the rows of Wg-expressing cells. This setup allows for a direct comparison of the levels of free Wg within the stripe to that in the adjacent cells. In the case of passive protection, we find that the distribution of free ligand outside the ectopic stripe is the same as that within the stripe (Figure 5A). Indeed, under steady-state conditions, the flux of dissociated ligand is precisely balanced by the flux of associated ligand. In contrast, in the case of active stabilization, the diffusion length of the free ligand is enhanced by the presence of receptor, allowing it to move further inside the stripe. Moreover, an asymmetry in free ligand level is generated between the stripe and the adjacent regions, leading to a net flow of ligand from the stripe, resulting in a wedge-like distribution of free ligand that peaks at the center of the ectopic stripe (Figure 5B). Note also that conversely, if receptor-mediated endocytosis is a major factor in ligand degradation, the diffusion length of free ligand is in fact reduced in the presence of receptors, leading to an inward flow of ligand from the external regions (Figure 5C). Importantly, since free and receptor-bound Wg are at equilibrium, altered diffusion length of free Wg within the stripe is reflected also in the distribution of receptor-bound Wg, which is significantly easier to detect experimentally (Figures 5A–5C). We have also verified that the wedge-like shape in Wg distribution is unique to the model of active stabilization and does not appear as a transient state in the other cases. (See Supplemental Data, section 3 for more detailed discussion.)

The distribution of receptor-bound Wg within the stripe of ectopic receptor expression can thus be used to test if Wg is actively stabilized by its receptor. Previous experiments examined situations of high receptor levels, by ectopically expressing the extracellular domain of DFz2, anchored to the cell surface via a glycerol-phosphatidylinositol linkage (GPI-Dfz2) (Cadigan et al., 1998). A non-cell-autonomous increase in free Wg was observed, reflected by an elevation in endocytotic Wg vesicles in cells adjacent to the GPI-DFz2-expressing cells (Cadigan et al., 1998; Rulifson et al., 2000). Those experiments, however, led to the stabilization of Wg throughout the pouch and were thus not sufficient for elucidating the pattern of Wg distribution. To generate lower levels of Wg stabilization, we induced ectopic receptor expression in a stripe perpendicular to normal Wg expression using the intermediate-level driver *dpp-Gal4*. An accumulation of Wg within the GPI-DFz2 stripe which displayed a clear wedge-like pattern was observed (Figures 5D–5G). Neither the wedge-like shape of Wg accumulation within the stripe nor the non-cell-autonomous increase in Wg seen previously (Cadigan et al., 1998) are consistent with the receptor passively protecting the bound Wg from degradation but point to the involvement of active stabilization of the free Wg. Those results are thus consistent with the theoretical proposal that DFz2 plays an active role in stabilizing free Wg.

It should be noted that, since GPI-DFz2 functions as a dominant-negative receptor (Rulifson et al., 2000), our results are also consistent with an alternative interpretation whereby Wg signaling enhances the degradation
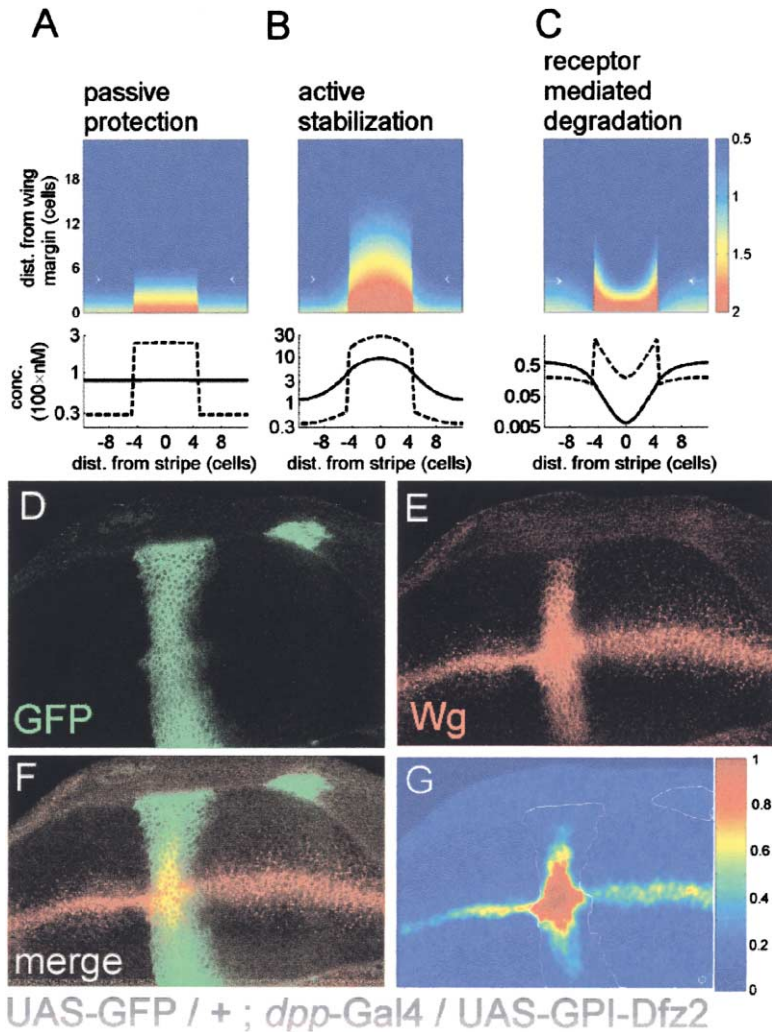
Figure 5. Distribution of Wg Can Identify Effects of the Receptors on the Ligand

Mathematical simulations were used to define how the distribution of Wg is affected by different facets of interactions with the receptor. Morphogen was produced at a constant rate in a line positioned at x = 0, and receptors were overexpressed in a perpendicular stripe of eight cells centered at y = 0. Three models were considered, corresponding to the situation of (A) passive protection (receptor-bound morphogen is protected from degradation), (B) active stabilization (receptor reduces degradation rate of free morphogen), and (C) enhanced degradation of receptor-bound morphogen (e.g., morphogen is degraded through receptor-mediated endocytosis). The upper panel presents the results of two-dimensional simulation, while the lower panel shows the one-dimensional distribution along a line parallel to the Wg-expressing cells (the cross section is indicated by arrows). In all models, morphogen accumulates on the overexpressing cells. However, the shape of this accumulation depends on the model used. In the case of active stabilization, morphogen accumulates in a wedge-like pattern which peaks at the center of the ectopic stripe. Note that a slight increase in the level of free ligand is observed also in cells nearby the stripe. Both aspects are unique to the case of active stabilization but are not observed when passive protection is used. (D–G) Experimental measurements of Wg accumulation following ectopic receptor expression. (D–F) dpp-Gal4 driver was used to express membrane-anchored GPI-Dfz2 in a stripe perpendicular to the normal Wg expression domain. Stripe boundaries were labeled using the UAS-CD8-GFP reporter. Wing-imaginal discs from third star larvae were stained for GFP (green) and for Wg (red). Receptor-bound Wg shows a wedge-like shape within the stripe of ectopic GPI-Dfz2. This indicates that DFz2 stabilizes free Wg. (G) Quantitation of Wg staining. Full line indicates the stripe boundaries (defined as the point where anti-GFP staining decreases to 20% of its maximum). Note that within the domain where the wedge of Wg distribution is formed, expression levels of the driver (as reflected by GFP expression), appear uniform. Thus, the wedge cannot be accounted for simply by graded expression of the receptor within the stripe.

of free Wg, e.g., by a transcriptional induction of a protease. Such a mechanism would also increase Wg degradation close to its source, thus enhancing the system robustness through the same mechanism of self-enhanced ligand degradation.

Hh-Ptc Interaction in the Drosophila Wing Disc

The other class of robust networks that were identified by the numeric screen is characterized by two features. First, receptor expression is upregulated by morphogen signaling. Second, morphogen is degraded primarily through receptor-mediated endocytosis. Both properties appear to be used by the Hh system during the patterning of the Drosophila wing disc. Hh is expressed in the posterior compartment of the wing disc. It was reported that Hh signaling induces the expression of its receptor Patched (Ptc) (Chen and Struhl, 1996). The significance of this induction for Hh-mediated patterning is highlighted by the fact that this feedback is observed in all systems where Hh functions (Chuang and Kornberg, 2000). In addition, following the binding of Hh to

Ptc, the complex undergoes endocytosis leading to the degradation of both Hh and Ptc (Incardona et al., 2002). It is likely that this mechanism plays a prominent role in Hh degradation since overexpression of Ptc significantly reduces Hh signaling range (Chen and Struhl, 1996).

Upon examining the signaling profile generated by the Hh-like class of networks, we noticed that the steady-state profile displays a discontinuity with a practically all-to-none transition at a particular spatial position (Figure 6A). Theoretical study confirmed that this bistability is a general feature of the model, resulting from a positive feedback loop controlling receptor levels (increasing signaling levels induces receptor expression, which in turn further enhances signaling; see inset to Figure 6A). Due to this positive feedback, the only possible steady states correspond to minimal or maximal signaling. The usefulness of such a bistable system for generating long-range patterning is doubtful.

The difficulty of the model in generating graded signaling indicates that it does not capture the essence of
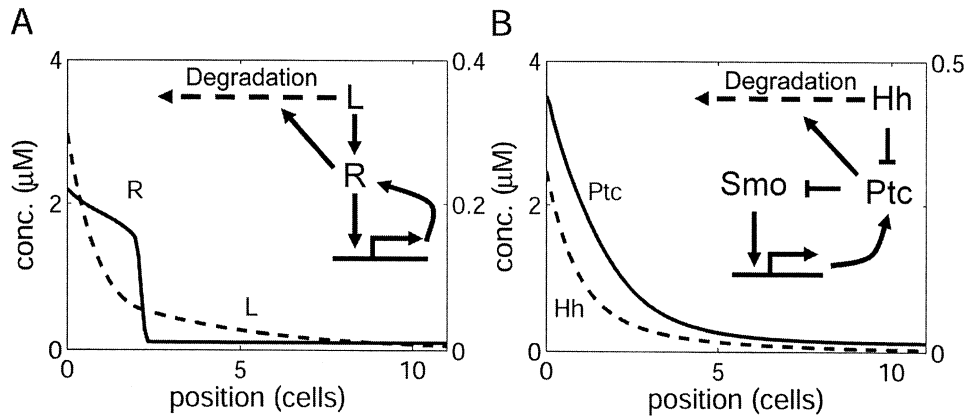
Figure 6. Bistable and Graded Signaling Profile Generated by Positive Feedback on Receptor Expression

Numerical simulation comparing signaling through receptor activation (A) with signaling through the release of inhibition (B). In both models, morphogen signaling induces receptor expression. The models are depicted schematically in the inset; see Experimental Procedures for equations and parameters.

the Hh morphogen system. An aspect which was not included in our analysis is the requirement of the transmembrane protein Smoothened (Smo) in transducing the signal (Alcedo et al., 1996; van den Heuvel and Ingham, 1996). Smo has an intrinsic signaling activity and is capable of inducing Hh-responsive genes. Ptc inhibits Smo signaling, but this inhibition is relieved upon Hh binding. The mechanisms by which Ptc affects Smo are not clear. Smo was initially implicated as a coreceptor for Ptc. Recent findings suggest that Ptc regulates Smo activity indirectly (Denef et al., 2000). Other reports have demonstrated colocalization of Ptc and Smo prior to signaling and had shown that upon Hh binding Smo is endocytosed together with Ptc. Smo is segregated from Ptc and Hh only later in the process, prior to their degradation (Incardona et al., 2002; Stark, 2002).

Extending our model to include Smo, we found that graded signaling is retrieved; indicating that the positive feedback loop of Ptc expression was broken (Figure 6B). Indeed, since Ptc inhibits the intrinsic signaling activity of Smo, increase in Ptc levels can only reduce, rather than enhance, signaling. Under certain conditions (see Supplemental Data, section 4), signaling through the release of inhibition indeed maintains graded signaling and ensures robustness to fluctuations in morphogen production rate.

Discussion

Differential Decay of Morphogen Gradients

To induce several cell fates across a developing field, morphogen gradients should extend to considerable distances from their source. At the same time, to overcome biological fluctuations, the local morphogen level at a given position (e.g., at the future boundary between alternative cell fates) should be insensitive to the rate of morphogen production. A central result which emerged from our study is that those two requirements pose competing constraints on the shape of the morphogen gradient. While the latter favors a rapid decay close to

the source, the former requires that morphogen levels decrease slowly across the developmental field.

Models of morphogen gradients generally assume that morphogen concentration decays exponentially. This is indeed the case for a single diffusing morphogen undergoing linear degradation. Exponential decays are characterized by a single parameter: their decay length, λ, which defines the working range of the morphogen. To reach sufficient distances, λ should be comparable to size of the developing field. However, we have shown that λ also controls the robustness of the profile to variations in the rate of morphogen production. In fact, to buffer such fluctuations, λ should be significantly smaller than the size of the developing field (Figure 1). Obviously, exponential profiles cannot comply with both requirements.

We argue that biologically relevant morphogen gradients should possess at least two length scales: a rapid decay (short length scale) close to morphogen source and a slow decay (long length scale) further from the source. In fact, for the case of a single morphogen diffusing in a naive field, we have shown that this requirement is essential for achieving robustness, irrespective of the type of interactions between the morphogen and other (localized) components of the system (see Supplemental Data, section 1).

Our analysis focused on a canonical example of a single morphogen secreted from a localized source. Other mechanisms could function to ensure robustness in more complex systems (Eldar et al., 2002; Houchmandzadeh et al., 2002). Several alterative mechanisms, such as an inhibitor gradient generated from the opposite side of the tissue or coupling of patterning to tissue growth, were proposed, but their properties were not yet studied rigorously. It would be interesting to analyze general properties of such systems in order to infer additional principles that may be utilized for ensuring robustness. Finally, we note that our study focuses on extracellular mechanisms which generate robustness to fluctuations in the rate of morphogen secretion. Additional intracellular mechanisms could function within the
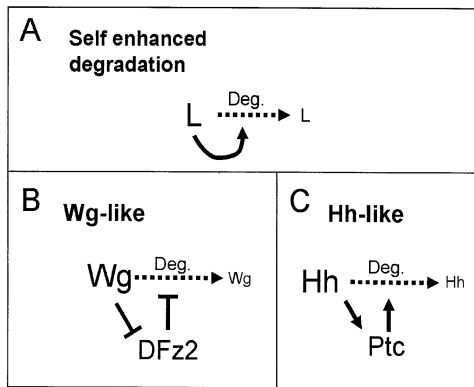
Figure 7. Modes of Achieving Robust Morphogen Patterning

(A) Self-enhanced morphogen degradation may present a general means for achieving robustness.
(B) In the Wg-like class of robust networks, morphogen signaling represses receptor expression, while receptor stabilizes the morphogen.
(C) In the Hh-like class of robust networks morphogen signaling activates receptor expression, while receptor enhances morphogen degradation. Both mechanisms thus ensure robustness using the same principle of enhancing ligand degradation in regions of high-morphogen levels.

restricted domain where ligand is produced to buffer morphogen secretion rates against fluctuation in its gene dosage.

We have also limited the discussion to mechanisms that provide robustness to the rate of morphogen secretion, but did not consider robustness to other parameters, such as receptor levels of diffusion rates. Robustness to receptor levels was demonstrated in the Wg system, for example, where it was shown that a normal wing is developed upon eliminating the signaling activity of one of the two alternative Wg receptors DFz or DFz2 (Chen and Struhl, 1999). Further analysis will be required for identifying mechanisms that ensure robustness to those additional factors.

Molecular Mechanisms Generating Differential Morphogen Decay
Differential morphogen decay is obtained under very general sets of conditions. In fact, any feedback which enhances the rate of morphogen degradation in regions of high morphogen concentrations can be used. To achieve robustness, the region where such feedback is effective need not to extend over the whole developmental field but may be confined only to the vicinity of the source.

We examined the validity of differential degradation rates to morphogen systems that pattern the *Drosophila* wing imaginal disc. Two of the morphogens functioning in the disc, Wg and Hh, are degraded at higher rates close to their source, in accordance with the robust mechanism. In both cases, different degradation domains are defined through reciprocal interactions between ligand and receptor (Figure 7).

Our analysis focused on the role of ligand-receptor interactions in shaping morphogen gradients. For simplicity, we did not include other aspects, such as feedback on protease expression, which may play a role in

actual morphogen systems. For example, HSPGs are modulators of morphogen signaling. In the *Drosophila* wing disc, the glycican Dally-like (Dlp) has been shown to stabilize Wg (Baeg et al., 2001; Strigini and Cohen, 2000), and this stabilization can be overcome by a secreted protein, Notum/Wingful (Gerlitz and Basler, 2002; Giraldez et al., 2002). Interestingly, Notum expression is induced by Wg signaling, again reducing Wg stability in regions of high Wg signaling (Gerlitz and Basler, 2002; Giraldez et al., 2002). It is likely that several layers function together to ensure robustness. Such mechanisms can readily be evaluated with respect to their compatibility with the general paradigm of self-enhanced ligand degradation.

Distinguishing Active Ligand Stabilization from Passive Protection
Negative feedback affecting morphogen stability emerged from our analysis as the key factor in ensuring robustness of morphogen gradients. Central to this mechanism is the ability to control the degradation of the free (diffusing) morphogen itself; for example, by altering the activity of a putative protease. However, in cases where such feedbacks were implied, morphogen stabilization was attributed only to the protection of bound morphogen from degradation (Cadigan et al., 1998; Rulifson et al., 2000).

We examined experimentally if DFz2 also stabilizes free Wg, by expressing membrane-anchored GPI-DFz2 in a stripe perpendicular to the region of Wg expression. Comparing the Wg profile between regions expressing normal and ectopic levels of receptors, we found that Wg accumulates in a wedge-like pattern that peaks at the center of the ectopic stripe, indicating that free Wg indeed diffuses further in the stripe region, where receptor levels are high. The wedge shape is generated by loss of free Wg to the cells adjacent to the stripe. The same effect may also account for the non-cell-autonomous increase in free Wg, reflected by an elevation in endocytotic Wg vesicles in cells adjacent to the GPI-DFz2 expressing cells, which was reported previously (Cadigan et al., 1998; Rulifson et al., 2000). We have verified that passive protection of receptor-bound Wg, or the transport of receptor-bound Wg through argosomes (Greco et al., 2001), cannot account for the wedge-like pattern of Wg accumulation and the non-cell-autonomous effects (see Supplemental Data, section 3.3). Both aspects of Wg accumulation are consistent with the proposal that DFz2 actively protects free Wg from degradation, as was predicted by our theoretical analysis.

Conclusions
Our work focused on the central role of the interaction between morphogens and their cognate receptors in shaping morphogen distribution and the resulting signaling gradients. Transcriptional regulation of receptor expression, coupled with the capacity of the receptor to modulate morphogen stability, can establish a morphogen profile which will buffer fluctuations in morphogen production rate. Such profiles are established when ligand degradation rate is enhanced in regions of high-morphogen levels. Self-enhanced ligand degradation may thus represent a general mechanism for ensuring the robustness of long-range morphogen gradients.

Experimental Procedures

Fly Strains and Immunostaining

To ectopically express DFz2 in the wing disc, flies carrying UAS-GPI-DFz2 (Cadigan et al., 1998) were crossed to dpp-Gal4 flies (described by Wilder and Perrimon, 1995). These flies also carried UAS-CD8-GFP (Lee and Luo, 1999), to mark the domain of Gal4 expression. Flies were raised at 25°C. Third instar larvae were dissected, and whole-mount immounostaining was carried out according to standard methods. The antibodies used were mouse anti-Wg (Brook and Cohen, 1996) and rabbit anti-GFP (Santa Cruz). Fluorescent secondary antibodies were from Jackson ImmunoResearch.

Numerical Screen

The general model used in the numeric screen (Figure 2) was defined by the following set of reaction-diffusion equations:

$$\frac{\partial\{L\}}{\partial t} = D\frac{\partial^2\{L\}}{\partial x^2} - k^1_+\{R\}\{L\} + k^1_-\{RL\} - a_1\{RP\}\{L\}$$

$$- a_2\{P\}\{L\} - a_3\{L\}$$

$$\frac{\partial\{RL\}}{\partial t} = k^1_+\{R\}\{L\} - k^1_-\{RL\} - a_4\{RL\}$$

$$\frac{\partial\{RP\}}{\partial t} = k^2_+\{R\}\{P\} - k^2_-\{RP\}$$

$$\frac{\partial\{R\}}{\partial t} = \eta_{r1}\frac{K_a^m}{K_a^m + \{RL\}^m} + \eta_{r2}\frac{\{RL\}^n}{K_b^n + \{RL\}^n}$$

$$- k^2_+\{R\}\{P\} + k^2_-\{RP\}$$

$$- k^1_+\{R\}\{L\} + k^1_-\{RL\} - \alpha_5\{R\} + \rho\alpha_4\{RL\}$$

$$P^{tot} = \{P\} + \{RP\},$$

where $\{L\}$, $\{R\}$, and $\{P\}$ denote the concentrations of the ligand, receptor, and protease, respectively, and complexes are denoted by their constituents.

We have nondimensionalized and solved those equations in a region $0 < x < 1$, assuming a constant flux as the left boundary condition ($D\nabla L = \eta_L$ at $x = 0$) and $D\nabla L = 0$ at $x = 1$. At each run, all parameters were chosen randomly, as described in the Supplemental Data. To measure robustness, we first measured the threshold level of ligand L_{th} found at the cell fate boundary $x = 0.5$. We then reduced by 2-fold the ligand production rate at the boundary $\lambda_L^{new} = \lambda_L/2$ and solved the system again with this altered boundary condition. Robustness was quantified by the ratio between the observed shift in cell fate (denoted by δx) and the shift that would have been obtained by an equivalent exponential system:

$$\text{Robustness} = \frac{x_2 - x_1}{\log(L(x_1)/L(x_2))}\delta x^{-1}, \text{ where } x_1 = 0.1; x_2 = 0.6.$$

For more details about the choice of this measure, see Supplemental Data.

The parameters used for defining the axes in Figure 3E are defined as:
x axis,

$$R_{prod} = \sigma(\log_{10}(\Omega_+ + \Omega_-)) \cdot g(\max(\Omega_+))$$

$$- \max(\Omega_-)); \quad g(x) = \begin{cases} 1 & x > 0 \\ -1 & x < 0 \end{cases}$$

and y axis,

$$R_{deg} =$$

$$\log_{10}\left[\frac{\left\langle\alpha_1\frac{\{R\}}{K_P + \{R\}} + \alpha_2 h\left(\frac{K_P}{\{R\}}\right) + \alpha_3 + \alpha_4 R\right\rangle}{\left\langle\alpha_1 h\left(\frac{\{R\}}{K_P}\right) + \alpha_2\frac{K_P}{K_P + \{R\}} + \alpha_3\right\rangle}\right];$$

$$h(x) = \begin{cases} 1 & x > 1 \\ 0 & x < 1 \end{cases}$$

where $\langle\ \rangle, \sigma$ denote the average and standard deviation of the appropriate term, and $\Omega_{+/-}$ are the positive and negative regulation elements;

$$\Omega_- = \eta_{r1}\frac{K_a^m}{K_a^m + (\{R\}\{L\})^m}; \ \Omega_+ = \eta_{r2}\frac{(\{R\}\{L\})^n}{K_b^n + (\{R\}\{L\})^n}.$$

See Supplemental Data for more details.

Wingless Model

The models used for simulating the Wg morphogen system were defined by the following set of reaction-diffusion equation:

$$\frac{\partial\{Wg\}}{\partial t} = D\frac{\partial^2\{Wg\}}{\partial x^2} - k^{fw}_+\{DFz2\}\{Wg\}$$

$$+ k^{fw}_-\{WgDFz2\} - \lambda\{Wg\}\{X\}$$

$$\frac{\partial\{DFz2\}}{\partial t} = \eta_{Fz}\frac{K_t^m}{K_t^m + \{WgDfz2\}^m} - \alpha\{DFz2\}$$

$$- k^{fw}_+\{DFz2\}\{Wg\} + k^{fw}_-\{WgDFz2\}$$

$$- k^{fx}_+\{DFz2\}\{X\} + k^{fx}_- \{XDFz2\}$$

$$+ \alpha\chi\rho\{WgDFz2\}$$

$$\frac{\partial\{WgDFz2\}}{\partial t} = k^{fw}_+\{DFz2\}\{Wg\} - k^{fw}_-\{WgDFz2\}$$

$$- \alpha\chi\{WgDFz2\}$$

$$\frac{\partial\{XDFz2\}}{\partial t} = k^{fx}_+ \{DFz2\}\{X\} - k^{fx}_-\{XDFz2\}$$

$$X^{tot} = \{X\} + \{XDFz2\}$$

where $\{Wg\}$, $\{DFz2\}$, and $\{X\}$ denote the levels of Wg, DFz2, and a putative protease, respectively, and complexes are denoted by their constituents. We assume that Wg flux at $x = 0$ is equal to $\eta_{Wg}L_p$. Passive protection is defined by the following parameters: $D = 0.1$ $\mu m^2 s^{-1}$, $k^{fw}_+ = 6.7 \cdot 10^{-3}$ $\mu M^{-1}s^{-1}$, $k^{fw}_- = 3.3 \cdot 10^{-3}s^{-1}$, $\lambda = 3.7 \cdot 10^{-2}$ $\mu M^{-1}s^{-1}$, $\eta_{Wg} = 2.4 \cdot 10^{-3}$ $\mu M \cdot s^{-1}$, $L_p = 4.5$ μm, $\eta_{Fz} = 1.7 \cdot 10^{-3}$ $\mu M \cdot s^{-1}$, $K_t = 2 \cdot 10^{-3}$ μM, $n = 1.5$, $\alpha = 3.3 \cdot 10^{-4}s^{-1}$, $k^{fx}_+ = 0$ $\mu M^{-1}s^{-1}$, $k^{fw}_- = 3.3 \cdot 10^{-4}s^{-1}$, $\chi = 0$, $\rho = 0$, $X^{tot} = 0.3$ μM. The field size is $L = 75$ μm. Each cell is 3 μm length. We assume a sink at the end of the wing disc.

Active stabilization is defined by the same set of equations but setting the following parameters differently: $k^{fx}_+ = 0.16$ $\mu M^{-1}s^{-1}$, $\eta_{Wg} = 4.4 \cdot 10^{-2}$ $\mu M \cdot s^{-1}$, $\lambda = 1.4 \cdot 10^{-2}s^{-1}$. The linear profile has the same concentration as the nonlinear at distances of 7 and 17 cells from the source. See Supplemental Data for more information.

Two-dimensional simulations are solved with similar equations on a two-dimensional lattice. Receptor levels are upregulated along an eight cell wide stripe, perpendicular to the Wg source. We also assume that recycling is inefficient along the stripe. Overexpression is simulated by assigning a constant production rate to the receptor, independent of Wg inhibition. Outside the stripe we use the same equations as for the one-dimensional simulations. Active stabilization (Figure 5B) is set by assigning $D = 0.1$ $\mu m^2 s^{-1}$, $k^{fw}_+ = 6.7 \cdot 10^{-3}$ $\mu M^{-1}s^{-1}$, $k^{fw}_- = 3.3 \cdot 10^{-3}s^{-1}$, $\lambda = 3.7 \cdot 10^{-2}$ $\mu M^{-1}s^{-1}$, $\eta_{Wg} = 7.4 \cdot 10^{-3}$ $\mu M \cdot s^{-1}$, $L_p = 4.5$ μm, $\eta_{Fz} = 1.7 \cdot 10^{-4}$ $\mu M \cdot s^{-1}$, $K_t = 2 \cdot 10^{-3}$ μM, $n = 1.5$, $\alpha = 3.3 \cdot 10^{-4}s^{-1}$, $k^{fx}_+ = 0.41$ $\mu M^{-1}s^{-1}$, $k^{fx}_- = 3.3 \cdot 10^{-4}s^{-1}$, $\chi = 0$, $\rho = 0$, $X^{tot} = 0.3$ μM. Within the stripe, we use the same parameters except for $\chi = 0.1$ and receptor production rate, $\eta_{Fz} = 5.1 \cdot 10^{-3}$ $\mu M \cdot s^{-1}$. Passive protection model (Figure 5A) is set by assigning $k^{fx}_+ = 1.6 \cdot 10^{-5}$ $\mu M^{-1}s^{-1}$, $X^{tot} = 0.75$ μM. Receptor-mediated endocytosis model is obtained by assigning $k^{fx}_+ = 1.6 \cdot 10^{-5}$ $\mu M^{-1}s^{-1}$, $X^{tot} = 0.15$ μM, $\chi = 1$.

Hedgehog Model

Hedgehog simple model, where signaling depends on Ptc-Hh complex, is solved with the equations

$$\frac{\partial \{Hh\}}{\partial t} = D\frac{\partial^2 \{Hh\}}{\partial x^2} - k_+^{ph}\{Hh\}\{Ptc\} + k_-^{ph}\{PtcHh\}$$

$$\frac{\partial \{Ptc\}}{\partial t} = \eta_{Ptc}^{end} + \eta_{Ptc}^{reg}\frac{\{PtcHh\}^n}{K_t^n + \{PtcHh\}^n}$$

$$- \alpha_P\{Ptc\} - k_+^{ph}\{Hh\}\{Ptc\} + k_-^{ph}\{PtcHh\}$$

$$\frac{\partial \{PtcHh\}}{\partial t} = k_+^{ph}\{Hh\}\{Ptc\} - k_-^{ph}\{PtcHh\}$$

$$- \alpha_{ph}\{PtcHh\},$$

where $\{Hh\}$, $\{Ptc\}$, and $\{PtcHh\}$ are the appropriate levels of the proteins and the complex. We assume that Hh flux at $x = 0$ is equal to $\eta_{Hh}L_P$. The parameters used are: $D = 1 \ \mu m^2 s^{-1}$, $k_+^{ph} = 7.15 \cdot 10^{-2}$ $\mu M^{-1}s^{-1}$, $k_-^{ph} = 6.25 \cdot 10^{-4} s^{-1}$, $\eta_{Ptc}^{end} = 6.2 \cdot 10^{-5} \ \mu M \cdot s^{-1}$, $\eta_{Ptc}^{reg} = 1.1 \cdot 10^{-3}$ $\mu M \cdot s^{-1}$, $\alpha_P = 6.25 \cdot 10^{-4} s^{-1}$, $\alpha_{PH} = 6.9 \cdot 10^{-2} s^{-1}$, $\eta_{Hh} = 3.3 \cdot 10^{-3} \ \mu M \cdot s^{-1}$, $L_p = 30 \ \mu m$, $K_t = 4.8 \cdot 10^{-2} \ \mu M$; $n = 3$.

The model incorporating Smoothened is described by the equations

$$\frac{\partial \{Hh\}}{\partial t} = D\frac{\partial^2 \{Hh\}}{\partial x^2} - k_+^{psh}\{Hh\}\{PtcSmo\}$$

$$+ k_-^{psh}\{PtcSmoHh\} - k_+^{ph}\{Hh\}\{Ptc\}$$

$$+ k_-^{ph}\{PtcHh\}$$

$$\frac{\partial \{Ptc\}}{\partial t} = \eta_{Ptc}^{end} + \eta_{Ptc}^{reg}\frac{\{PtcSmoHh\}^n}{K_t^n + \{PtcSmoHh\}^n}$$

$$- \alpha_P\{Ptc\} - k_+^{ph}\{Hh\}\{Ptc\}$$

$$+ k_-^{ph}\{PtcHh\} + \rho\alpha_{ph}\{PtcHh\}$$

$$- k_+^{ps}\{Ptc\}\{Smo\} + k_-^{ps}\{PtcSmo\}$$

$$\frac{\partial \{PtcHh\}}{\partial t} = k_+^{ph}\{Hh\}\{Ptc\} - k_-^{ph}\{PtcHh\}$$

$$- \alpha_{ph}\{PtcHh\}$$

$$\frac{\partial \{PtcSmo\}}{\partial t} = k_+^{ps}\{Ptc\}\{Smo\} - k_-^{ps}\{PtcSmo\}$$

$$- k_+^{psh}\{Hh\}\{PtcSmo\}$$

$$+ k_-^{psh}\{PtcSmoHh\}$$

$$\frac{\partial \{PtcSmoHh\}}{\partial t} = k_+^{psh}\{Hh\}\{PtcSmo\}$$

$$- k_-^{psh}\{PtcSmoHh\}$$

$$Smo^{tot} = \{Smo\} + \{PtcSmo\} + \{PtcSmoHh\},$$

where Smo concentration is denoted by $\{Smo\}$ and complexes are denoted by their constituents. The following parameters were used: $D = 1 \ \mu m^2 s^{-1}$, $k_+^{ph} = 7.15 \cdot 10^{-2} \ \mu M^{-1}s^{-1}$, $k_-^{ph} = 6.25 \cdot 10^{-4} s^{-1}$, $\eta_{Ptc}^{end} = 6.2 \cdot 10^{-5} \ \mu M \cdot s^{-1}$, $\eta_{Ptc}^{reg} = 1.1 \cdot 10^{-3} \ \mu M \cdot s^{-1}$, $\alpha_P = 6.25 \cdot 10^{-4} s^{-1}$, $\alpha_{PH} = 2 \cdot 10^{-2} s^{-1}$, $\eta_{Hh} = 3.3 \cdot 10^{-3} \ \mu M \cdot s^{-1}$, $L_p = 30 \ \mu m$, $K_t = 5.7 \cdot 10^{-2}$ μM, $n = 2$, $\rho = 1$, $k_+^{ps} = 1.25 \ \mu M^{-1}s^{-1}$, $k_-^{ps} = 6.25 \cdot 10^{-4} s^{-1}$, $k_+^{psh} = 2.1 \cdot 10^{-3} \ \mu M^{-1}s^{-1}$, $k_-^{psh} = 6.25 \cdot 10^{-4} s^{-1}$, $Smo^{tot} = 0.3 \ \mu M$.

References

Alcedo, J., Ayzenzon, M., Von Ohlen, T., Noll, M., and Hooper, J.E. (1996). The *Drosophila* smoothened gene encodes a seven-pass membrane protein, a putative receptor for the hedgehog signal. Cell *86*, 221–232.

Baeg, G., Lin, X., Khare, N., Baumgartner, S., and Perrimon, N. (2001). Heparan sulfate proteoglycans are critical for the organization of the extracellular distribution of Wingless. Development *128*, 87–94.

Bellaiche, Y., The, I., and Perrimon, N. (1998). Tout-velu is a Drosophila homologue of the putative tumour suppressor EXT-1 and is needed for Hh diffusion. Nature *394*, 85–88.

Briscoe, J., and Ericson, J. (2001). Specification of neuronal fates in the ventral neural tube. Curr. Opin. Neurobiol. *11*, 43–49.

Brook, W.J., and Cohen, S.M. (1996). Antagonistic interactions between wingless and decapentaplegic responsible for dorsal-ventral pattern in the Drosophila Leg. Science *273*, 1373–1377.

Burke, R., Nellen, D., Bellotto, M., Hafen, E., Senti, K.-A., Dickson, B.J., and Basler, K. (1999). Dispatched, a novel sterol-sensing domain protein dedicated to the release of cholesterol-modified Hedgehog from signaling cells. Cell *99*, 803–815.

Cadigan, K.M. (2002). Regulating morphogen gradients in the Drosophila wing. Semin. Cell Dev. Biol. *13*, 83–90.

Cadigan, K.M., Fish, M.P., Rulifson, E.J., and Nusse, R. (1998). Wingless repression of *Drosophila* frizzled 2 expression shapes the wingless morphogen gradient in the wing. Cell *93*, 767–777.

Campbell, G., and Tomlinson, A. (1999). Transducing the Dpp morphogen gradient in the wing of *Drosophila*: regulation of Dpp targets by brinker. Cell *96*, 553–562.

Chen, Y., and Struhl, G. (1996). Dual roles for patched in sequestering and transducing Hedgehog. Cell *87*, 553–563.

Chen, C.M., and Struhl, G. (1999). Wingless transduction by the Frizzled and Frizzled2 proteins of Drosophila. Development *126*, 5441–5452.

Chuang, P.-T., and Kornberg, T.B. (2000). On the range of Hedgehog signaling. Curr. Opin. Genet. Dev. *10*, 515–522.

Denef, N., Neubuser, D., Perez, L., and Cohen, S.M. (2000). Hedgehog induces opposite changes in turnover and subcellular localization of patched and smoothened. Cell *102*, 521–531.

Dubois, L., Lecourtois, M., Alexandre, C., Hirst, E., and Vincent, J.P. (2001). Regulated endocytic routing modulates wingless signaling in *Drosophila* embryos. Cell *105*, 613–624.

Eldar, A., Dorfman, R., Weiss, D., Ashe, H., Shilo, B.Z., and Barkai, N. (2002). Robustness of the BMP morphogen gradient in Drosophila embryonic patterning. Nature *419*, 304–308.

Entchev, E.V., Schwabedissen, A., and Gonzalez-Gaitan, M. (2000). Gradient formation of the TGF-beta homolog Dpp. Cell *103*, 981–991.

Freeman, M. (2000). Feedback control of intercellular signaling in development. Nature *408*, 313–319.

Gerlitz, O., and Basler, K. (2002). Wingful, an extracellular feedback inhibitor of Wingless. Genes Dev. *16*, 1055–1059.

Giraldez, A.J., Copley, R.R., and Cohen, S.M. (2002). HSPG modification by the secreted enzyme Notum shapes the Wingless morphogen gradient. Dev. Cell *2*, 667–676.

Greco, V., Hannus, M., and Eaton, S. (2001). Argosomes: a potential vehicle for the spread of morphogens through epithelia. Cell *106*, 633–645.

Houchmandzadeh, B., Wieschaus, E., and Leibler, S. (2002). Establishment of developmental precision and proportions in the early Drosophila embryo. Nature *415*, 798–802.

Incardona, J.P., Gruenberg, J., and Roelink, H. (2002). Sonic hedgehog induces the segregation of patched and smoothened in endosomes. Curr. Biol. *12*, 983–995.

Jazwinska, A., Kirov, N., Wieschaus, E., Roth, S., and Rushlow, C. (1999). The *Drosophila* gene brinker reveals a novel mechanism of Dpp target gene regulation. Cell *96*, 563–573.

Kerszberg, M., and Wolpert, L. (1998). Mechanisms for positional

signalling by morphogen transport: a theoretical study. J. Theor. Biol. *191*, 103–114.

Lander, A.D., Nie, Q., and Wan, F.Y. (2002). Do morphogen gradients arise by diffusion? Dev. Cell *2*, 785–796.

Lecourtois, M., Alexandre, C., Dubois, L., and Vincent, J.P. (2001). Wingless capture by Frizzled and Frizzled2 in Drosophila embryos. Dev. Biol. *235*, 467–475.

Lecuit, T., and Cohen, S.M. (1997). Proximal-distal axis formation in the Drosophila leg. Nature *388*, 139–145.

Lecuit, T., Brook, W.J., Ng, M., Calleja, M., Sun, H., and Cohen, S.M. (1996). Two distinct mechanisms for long-range patterning by Decapentaplegic in the Drosophila wing. Nature *381*, 387–393.

Lee, T., and Luo, L. (1999). Mosaic analysis with a repressible cell marker for studies of gene function in neuronal morphogenesis. Neuron *22*, 451–461.

McDowell, N., and Gurdon, J.B. (1999). Activin as a morphogen in Xenopus mesoderm induction. Semin. Cell Dev. Biol. *10*, 311–317.

Morimura, S., Maves, L., Chen, Y., and Hoffmann, F.M. (1996). decapentaplegic overexpression affects Drosophila wing and leg imaginal disc development and wingless expression. Dev. Biol. *177*, 136–151.

Nellen, D., Burke, R., Struhl, G., and Basler, K. (1996). Direct and long-range action of a DPP morphogen gradient. Cell *85*, 357–368.

Neumann, C., and Cohen, S. (1997a). Morphogens and pattern formation. Bioessays *19*, 721–729.

Neumann, C.J., and Cohen, S.M. (1997b). Long-range action of Wingless organizes the dorsal-ventral axis of the Drosophila wing. Development *124*, 871–880.

Perrimon, N., and McMahon, A.P. (1999). Negative feedback mechanisms and their roles during pattern formation. Cell *97*, 13–16.

Roelink, H., Porter, J.A., Chiang, C., Tanabe, Y., Chang, D.T., Beachy, P.A., and Jessell, T.M. (1995). Floor plate and motor neuron induction by different concentrations of the amino-terminal cleavage product of sonic hedgehog autoproteolysis. Cell *81*, 445–455.

Rulifson, E.J., Wu, C.-H., and Nusse, R. (2000). Pathway specificity by the bifunctional receptor frizzled is determined by affinity for Wingless. Mol. Cell *6*, 117–126.

Stark, D.R. (2002). Hedgehog signalling: pulling apart patched and smoothened. Curr. Biol. *12*, R437–R439.

Strigini, M., and Cohen, S.M. (1997). A Hedgehog activity gradient contributes to AP axial patterning of the Drosophila wing. Development *124*, 4697–4705.

Strigini, M., and Cohen, S.M. (1999). Formation of morphogen gradients in the Drosophila wing. Semin. Cell Dev. Biol. *10*, 335–344.

Strigini, M., and Cohen, S.M. (2000). Wingless gradient formation in the Drosophila wing. Curr. Biol. *10*, 293–300.

Teleman, A.A., and Cohen, S.M. (2000). Dpp gradient formation in the *Drosophila* wing imaginal disc. Cell *103*, 971–980.

van den Heuvel, M., and Ingham, P.W. (1996). smoothened encodes a receptor-like serpentine protein required for hedgehog signalling. Nature *382*, 547–551.

Wilder, E.L., and Perrimon, N. (1995). Dual functions of wingless in the Drosophila leg imaginal disc. Development *121*, 477–488.

Wolpert, L. (1989). Positional information revisited. Development *107*, 3–12.

Zecca, M., Basler, K., and Struhl, G. (1996). Direct and long-range action of a wingless morphogen gradient. Cell *87*, 833–844.